CHEMISTRY
AN ASIAN JOURNAL

Accepted Article

Title: Redox Active Dynamic Self-supporting Thixotropic 3D-printable G-quadruplex Hydrogel

Authors: Apurba K Das, Ankan Biswas, Sayan Maiti, and Deepak Kalaskar

This manuscript has been accepted after peer review and appears as an Accepted Article online prior to editing, proofing, and formal publication of the final Version of Record (VoR). This work is currently citable by using the Digital Object Identifier (DOI) given below. The VoR will be published online in Early View as soon as possible and may be different to this Accepted Article as a result of editing. Readers should obtain the VoR from the journal website shown below when it is published to ensure accuracy of information. The authors are responsible for the content of this Accepted Article.

Redox Active Dynamic Self-supporting Thixotropic 3D-printable G-quadruplex Hydrogel

Ankan Biswas,[a] Sayan Maiti,[a] Deepak M. Kalaskar[b] and Apurba K. Das*[a]

[a]Department of Chemistry, Indian Institute of Technology Indore, Khandwa Road, Indore 453552, India. E-mail: apurba.das@iiti.ac.in

[b]Institute of Orthopaedics & Musculoskeletal Science, Division of Surgery and Intervention Science, Royal National Orthopaedic Hospital, University College London, Brockely Hill, Stanmore, Middlesex HA7 4LP, UK.

Abstract

Redox active G-quadruplex hydrogel was prepared by a dynamic boronate ester formation between ferroceneboronic acid and guanosine. Dynamic boronate esters built thixotropic and 3D-printability of the hydrogel. Initially, ferrocene moiety oxidized to produce weaker ferrocenium-based green hydrogel. However, less stable ferrocenium converted into more stable ferrocene to produce hydrophobic, water stable and robust hydrogel.

Keywords

G-quadruplex, Redox active hydrogel, Thixotropic, 3D-printable

1

Introduction

Development of hydrogels by molecular self-assembly is highly attractive for designing soft materials. Supramolecular hydrogels are applied in various fields including wound healing, tissue engineering, anti-bacterial agent, electrochromism, nanotechnology and sensing applications.[1-7] Hydrogels with injectable and self-healing properties restore their inherent elastic nature and possess quick gel-sol-gel transition. Fast gel-sol-gel transition produces several wide range of applications including 3D printing, drug release, electromagnetic shielding, supercapacitor.[8-11] Although low molecular weight (LMW) hydrogels have better homogeneity, reversibility and well tunable nature than polymeric hydrogels, LMW based 3D printable hydrogels are rare in literature and in very early stage of development.[8,12,13] Suitable building blocks and self-assembling strategy are required for the development of 3D printable hydrogels.

Guanosine and its derivatives are well known to form planner G-quartets among four molecules through Hoogsteen H-bonding.[14-15] Furthermore, these planner G-quartets build columnar, three dimensional nanofibrous G-quadruplex structure by π-π stacking interactions among aromatic purine rings.[15] Under certain experimental conditions, these nanofibrous networks encapsulate enough water to produce gel phase materials (G4 hydrogels). G-quadruplex structures are stabilized in presence of metal ions, especially in K^+ ions.[15] Previously, most of the studies about G4 hydrogels were mainly focused on investigation and understanding the supramolecular structure and stability in presence of different functional groups, ionic strength, metal ions, dyes and pHs.[16-20] Recently, G4 hydrogels have drawn great attraction in several wide range of applications in different fields.[8,13,21,22] Although G4 hydrogels have high potential for broad range of applications, there are several drawbacks of G4 hydrogels such as: i) requirement of excess amount of metal ions, ii) tendency of precipitation, iii) instability of gel phase due to hydrophilic nature of the gel, iv) poor solubility of guanosine and its analogues in water during preparation of the gel. Recently researchers are focused to overcome the challenges.
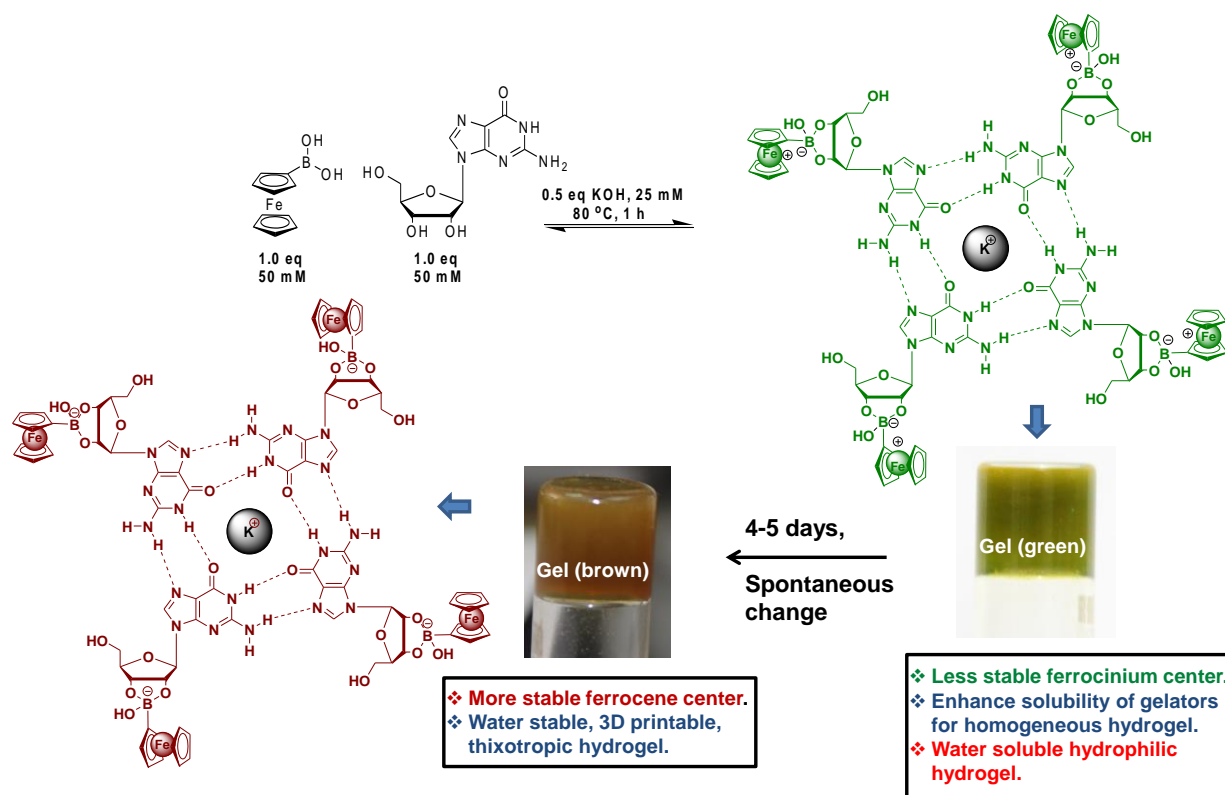
Scheme 1. Schematic representation for the preparation of ferrocene functionalized G-quadruplex hydrogel and spontaneous change from **gel (green)** to **gel (brown)** with their properties.

Different boronic acids or boric acid can bind with *cis*-1,2-diol of sugar moiety of guanosine to form boronate esters. Boronate ester mediated LMW G4 hydrogels are dynamic, self-healable and thixotropic in nature due to dynamic behaviour of boronic acid-boronate ester equilibrium in aqueous medium.[19,23,24]

Ferrocene-functionalized hydrogel can change its hydrophilicity and hydrophobicity by changing the oxidation state of Fe centre.[25] The oxidized hydrophilic ferrocinium is soluble in water. Neutral ferrocene is hydrophobic and insoluble in water due to presence of two hydrophobic cyclopentadienyl rings which can form stronger hydrogel.[26] Most of the reported ferrocene based hydrogels are stimuli responsive where redox behaviour is controlled by external stimuli.[26-29] Ferrocene-functionalized G4 system can provide interesting supramolecular architectures with different properties. Metal-free G-quartet and G-ribbon structures at solid-liquid interface with ferrocene-functionalized guanosine (at C-5′ position) have been reported.[30] Ferrocene-based hemin/G-quadruplex DNA

3

sequences also previously reported for analysis of DNA sequences.[31] Herein, we have prepared ferroceneboronate ester mediated G4 hydrogel.

Results and discussion

The G4 hydrogel was prepared by heating of ferroceneboronic acid (FcBA) and guanosine (G) in presence of aqueous KOH (Scheme 1) at 80 °C. The ratio (concentration) of G : FcBA : KOH is 1:1:0.5 (50 mM: 50 mM: 25 mM). During the preparation of the hydrogel, the solution turned green due to the oxidation of ferrocene to ferrocenium in presence of KOH. After cooling at room temperature, green hydrogel (**gel (green)**) was formed from the green solution. The observation is consistence with previous report by Hursthouse *et al.*, where ferroceneboronate ester of diols bound with anions followed by aerobic oxidation to yield green ferrocenium species.[32] However, ferrocenium (Fe(III)) has 17e, which is not stable. **Gel (green)** was spontaneously converted to brown, ferrocene-based 18e Fe(II) centre hydrogel (**gel (brown)**) (Figure 1a). Although the ferrocinium species is less stable, the initial oxidation produces ferrocinium ions, which are easily soluble during the gelation and have significant role to produce a homogeneous hydrogel. To study the role of aerobic oxygen for the initial oxidation of ferrocene, hydrogel was prepared in a round bottom flask under N_2 atmosphere. Under N_2 atmosphere, brown gel was formed due to lack of oxygen instead of formation of green ferrocenium species (Figure 1b). So, it is confirmed that initial oxidation was happening due to the presence of aerobic oxygen. However, exact electron transfer and reduction mechanism is not properly understood.

The pH of the hydrogel was ~7.8. To study the effect of pH on hydrogel with same ionic medium (K^+), KCl (neutral salt) and $KHSO_4$ (acidic salt) were used as K^+ source instead of KOH (basic). In both KCl (pH = 6.5) and $KHSO_4$ (pH = 4.0) medium, gel was not formed as the boronate ester formation is favoured at pH > 7 (Figure S1).[23] NaOH and LiOH were used to study the effect of other alkali metal ions on gelation at same pH. It was observed that weak gel was formed in presence of NaOH. In case of LiOH, viscous liquid was formed instead of the formation of hydrogel. The results reflect that K^+ ions are most suitable to fit inside G-quartets cavity to stabilize G-quadruplex structure and form strong hydrogel. On the other hand, Li^+ is too small to fit G-quartet structure due to

4

its smaller ionic radius and Na$^+$ moderately stabilizes the G-quadruplex structure. Here, strong hydrogel formation in presence of K$^+$ ions suggests that the hydrogel formation is going through G-quartets formation. Overall results suggest that the presence of suitable metal ions and pHs are crucial for the gelation.
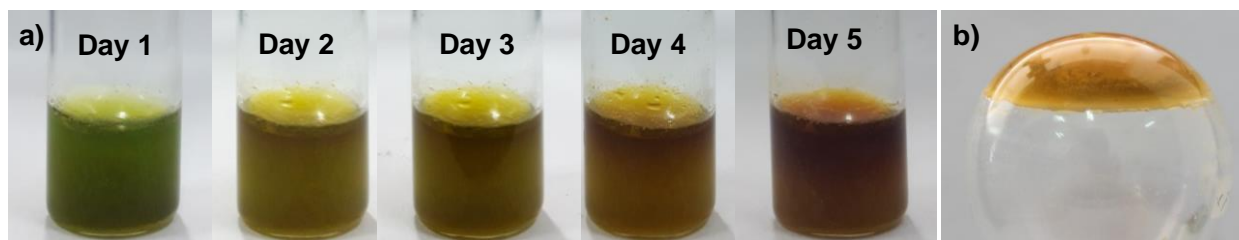

Figure 1. a) Spontaneous conversion of the **gel (green)** to **gel (brown)** at different time period. b) Hydrogel prepared in inert condition showing no oxidised green ferrocenium.
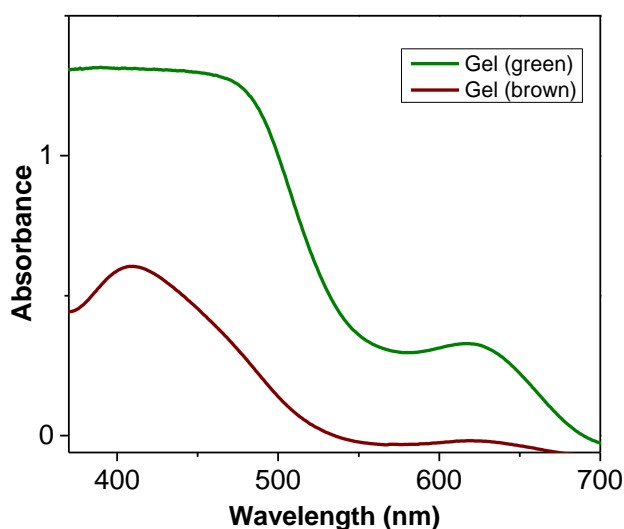

Figure 2. UV-Vis spectra of **gel (green)** and **gel (brown)** (25 mM, 25 ^{o}C).

The conversion from **gel (green)** to **gel (brown)** was taken about 5 days. The formation of ferrocenium in **gel (green)** was confirmed by UV-Vis spectra. Absorbance at 624 nm was observed, which is well known characteristic absorption peak for oxidized ferrocenium (Figure 2).[26] The **gel (brown)** shows absorbance at 407 nm for ferrocene centre (Figure 2).[26] However, the presence of trace amount of oxidised ferrocenium in

5

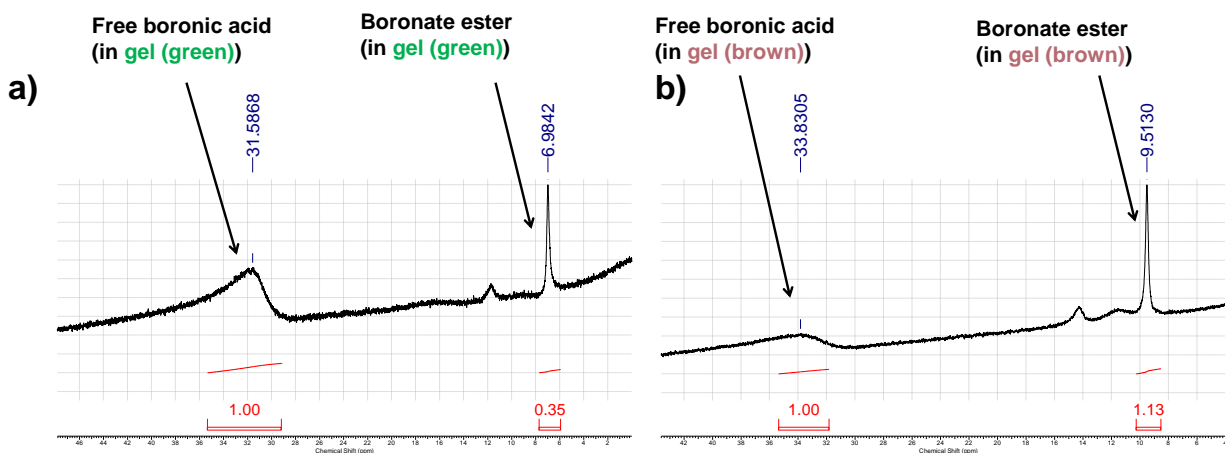the **gel (brown)** and ferrocene species in the **gel (green)** resulted in absorbance in UV-Vis spectra.

Figure 3. ^{11}B NMR of (a) **gel (green)** and (b) **gel (brown)** hydrogels (128 MHz, 10% D_2O).

The formation of boronate esters during gelation was confirmed by ^{11}B NMR. In aqueous medium, boronate esters exist in equilibrium between free boronic acids-boronate esters which are highly dependent on pH of the medium.[33] In aqueous conditions, ^{11}B NMR peak for free boronic acid is observed in downfield and after binding with *cis*-diols, a new peak is appeared at upfield for the formation of boronate esters.[8,34] ^{11}B NMR spectra of both ferrocene and ferrocinium boronic acids show chemical shift in the range of ~30-36 ppm depending upon the presence of other functional groups.[35] In our case, boronate ester peak was observed in 6.98 ppm with free acid peak in 31.58 ppm in the **gel (green)** (Figure 3a). In the **gel (brown)**, a peak at 9.51 ppm was attributed due to the presence of boronate ester with free acid peak at 33.83 ppm (Figure 3b). Chemical shift at upfield for both the free acid and ester in oxidised form (**gel (green)**) than in case of reduced **gel (brown)** was observed due to the paramagnetic effect of ferrocenium moiety. However, in case of **gel (green)** large paramagnetic shift in ^{11}B NMR was not observed for paramagnetic Fe(III) as 'B' atom is not directly bonded with Fe(III) atom.[35b,36]
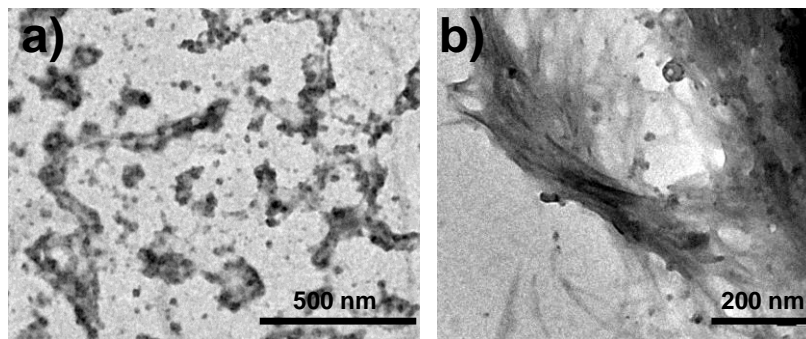
6

Figure 4. (a) TEM image of the **gel (green)** showing short and sparse fibers. (b) TEM image of the **gel (brown)** showing entangled nanofibers.

TEM images of the **gel (green)** showed short and spare fibers, due to ionic nature of the ferrocenium, however the **gel (brown)** exhibited entangled G-quadruplex nanofibers with average diameter of 20 nm and several micrometres in length (Figure 4). Circular dichroism (CD) is one of the effective tools to examine supramolecular secondary structures.[37,38,39] CD study was performed with the gels. Alternative positive negative bands around 300 nm are characteristic peaks for G-quadruplex structure.[19,20] In **gel (brown)**, an intense positive peak at 490 nm and a negative peak at 530 nm were attributed due to supramolecular chirality generated by ferrocene moiety.[27] An alternative positive peak at 301 nm and a negative peak at 281 nm were attributed to guanosine residue (Figure 5). In the **gel (green)**, single positive band at 510 nm was observed for ferrocene moiety and a negative band at 266 nm with low intense positive band at 300 nm were appeared due to guanosine moiety (Figure 5). CD study described that G-quadruplex formation in the **gel (brown)** is more prominent than in the **gel (green)**.
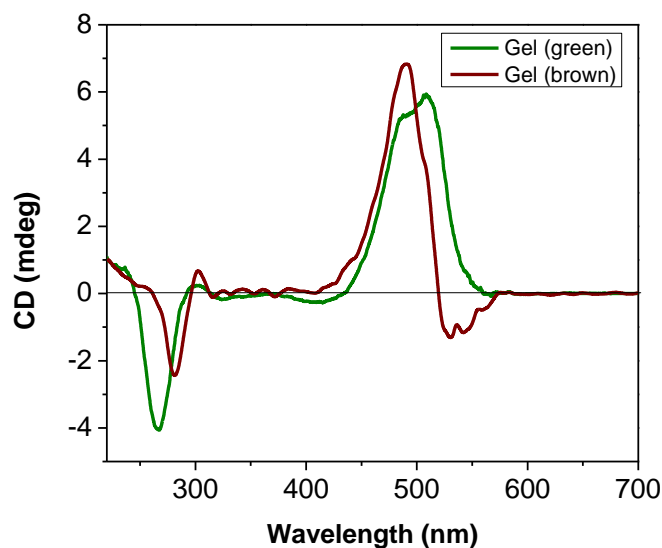
7

Figure 5. CD spectra of the **gel (green)** and **gel (brown)** (25 °C) showing the formation of G-quadruplex.

Formation of the G-quadruplex was further confirmed by PXRD study of the xerogel. The **gel (brown)** showed prominent peak at $2\theta = 27.65°$ which is associated with the characteristic π-π stacking interaction (~ 3.3 Å) between two G-quartets (Figure S2).[8] However, the **gel (green)** showed a broad peak in the region of $2\theta \approx 25$-$30°$ instead of the presence of any sharp peak.
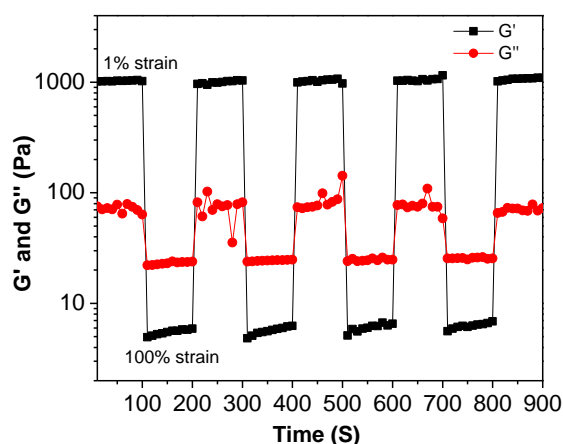

Figure 6. Cyclic dynamic strain sweep experiment of the **gel (brown)** showing shear thinning and thixotropic properties.

8

Rheological experiments were performed to obtain the mechanical properties of the gels. Frequency sweep experiments of both **gel (green)** and **gel (brown)** were carried out in the range of 100 rad/s to 0.05 rad/s at constant 1% strain. Throughout the experiments,
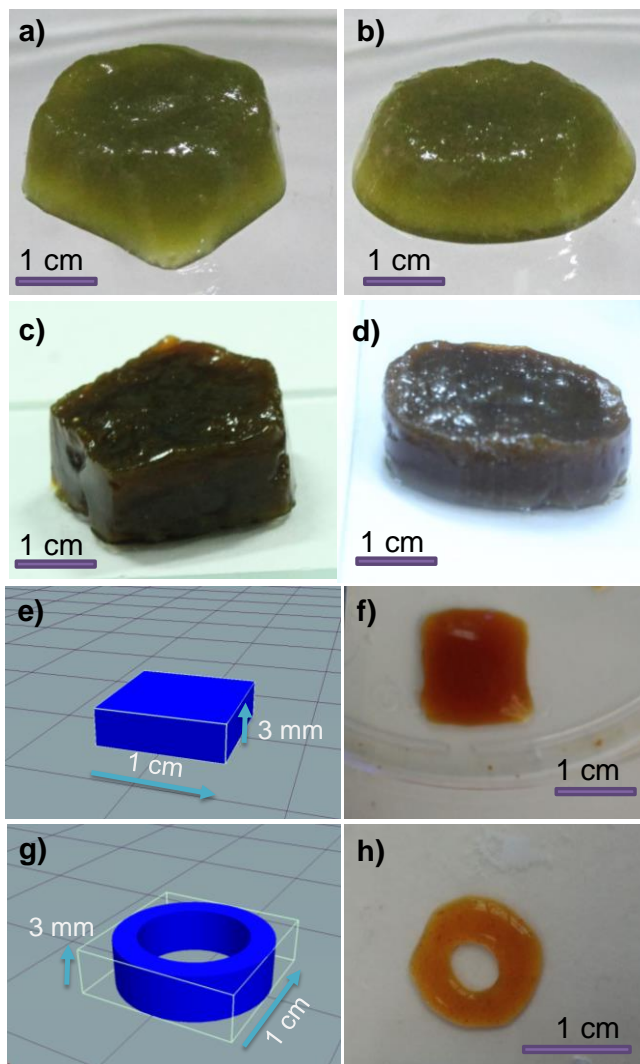

Figure 7. a) and b) Printed shape of syringe extruded **gel (green)**. c) and d) Printed shape of syringe extruded **gel (brown)**. c) CAD design of a 3D block (length = 1 cm, height = 3 mm) and d) 3D printed hydrogel. e) CAD design of a 3D circular structure (diameter = 1 cm, height = 3 mm) and f) 3D printed circular hydrogel structure.

storage modulus (G′) was higher than the loss modulus (G′′) assuring about the viscoelastic nature of the gels. G′ value of the **gel (green)** was ~500 Pa (at 10 rad/s), whether G′ value of the **gel (brown)** was ~1200 KPa (at 10 rad/s) (Figure S3). The study

represents that **gel (brown)** is more stepper, stronger than **gel (green)**. The **gel (brown)** was well injectable in nature. Cyclic dynamic strain sweep experiment was performed to investigate the self-healing and thixotropic properties of the **gel (brown)**. Alternative lower (1%) and higher (100%) strain were applied on the **gel (brown)**. At higher strain, the gel turned to sol state (G′<G′′) and after every successive step, the viscoelastic nature of the gel (G′>G′′) was quickly recovered from the sol state (Figure 6). The experiment was performed up to 9 cycles and almost 100% recovery of storage modulus was observed after 9 cycles.[40] So, the gel is highly thixotropic in nature and can be used for 3D printing.

Cyclic voltammetry experiment was carried out with the hydrogels. Both **gel (green)** and **gel (brown)** showed reversible peak under applied voltage (Figure S4). The **gel (green)** showed oxidation peak at 0.43 V and reduction peak at 0.27 V. In the **gel (grown)** form, oxidation peak shifted to 0.35 V and reduction peak shifted to 0.25 V. In CV experiments, no significant changes were observed. Oxidation and reduction peaks were observed due to the presence of ferrocenium and ferrocene species under applied voltage.[26]

Injectability, 3D-printability and structural rigidity of the **gel (brown)** was ensured by the rheological parameters. The **gel (green)** and **gel (brown)** were incorporated separately into syringe and different structures were printed by 22G needle (Figure 7a to 7d). In case of **gel (brown)**, the structures were stable to maintain its proper shape after printing (Figure 7b and 7c). However, when the **gel (green)** was printed, the sharp edges of the geometrical shapes were not clearly distinguishable like **gel (brown)** (Figure 7a and 7b). Moreover, liquid-like flow behaviours such as accommodation and spreading of the gels from the base of the printed shapes were observed (Figure 7a and 7b). So, the **gel (brown)** is more suitable for 3D-printing and has better shape supporting strength. The **gel (brown)** was put in a 3D-printer and different structures were printed according to predesigned "Computer Added Design'' (CAD) structure (Figure 7e to 7h). A 3D square block (length = 1 cm, height = 3 mm) and a 3D circular diagram (diameter = 1 cm, height = 3 mm) were designed and printed. Syringe pressure was adjusted as 13 KPa and 25G needle was use for printing purpose.

10

The **gel (green)** monolith was immersed into PBS buffer to check the stability of the hydrogel in aqueous medium. The **gel (green)** was soluble in buffer solution over a period of ~24h (Figure 8) due to its hydrophilic nature. However, the **gel (brown)** monolith was showing stability up to 30 days in buffer medium. After 30 days, degradation of the **gel (brown)** was observed at the bottom of the vial (Figure 8). The results show **gel (brown)** is highly stable in aqueous medium and has potential for diverse applications. Here, ferrocene moiety provides robust, water stable hydrogel by changing its oxidation state. Water stable 3D printable hydrogels have several applications. Moreover, this approach could be used to develop different ferrocene-based 3D printable water stable hydrogels for long term cell cultures and tissue growth, drug release and waste water remediation.
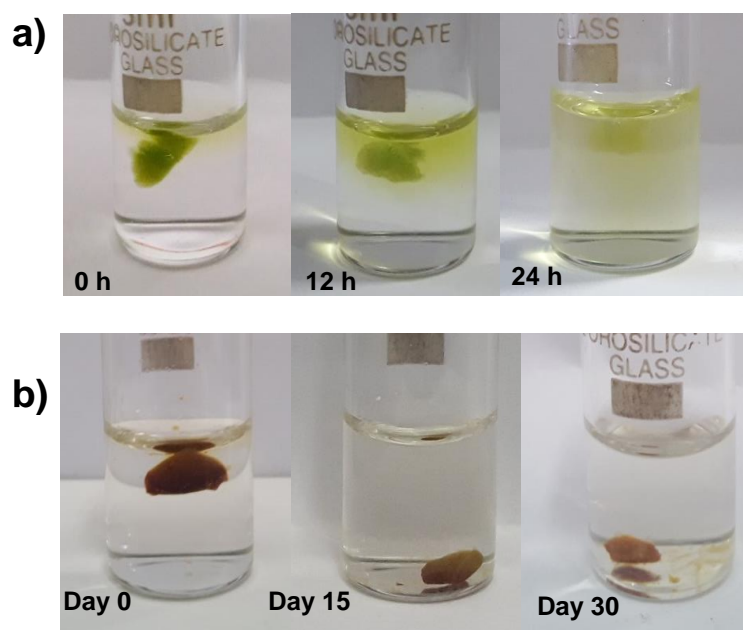

Figure 8. Water stability of the hydrogels in PBS buffer a) **gel (green)**, b) **gel (brown)** at different time period.

Conclusion

In conclusion, we have prepared ferroceneboronic acid functionalized dynamic redox active G-quadruplex hydrogel. Dynamic cyclic boronate ester of the gelators generates injectable and thixotropic behaviour of the gel. Initial oxidation of ferrocene to ionic ferrocenium helps to dissolve the gelators. After gelation, the less stable **gel (green)** was spontaneously converted to **gel (brown)** to achieve more stable 18e configuration in

11

Fe(II) centre and the gel became stronger, 3D printable and water stable. This new approach may help to synthesize water stable structures using 3D printing process for various applications.

Experimental section

General Methods:

All the chemicals were purchased from Sigma-Aldrich and Alfa Aesar and used without further purification. Milli-Q water was used for all the experiments and hydrogel preparation.

Preparation of hydrogel:

22.9 mg of ferroceneboronic acid (FcBA) and 28.3 mg of guanosine (G) were taken in a clean glass vial. 2 mL of 25 mM KOH solution was added into it. Then, the resulting mixture was kept under sonication for 4-5 minutes. After that, the vial was heated at 80 ℃ for 1 h (yellow color solution turned dark green solution) to solubilize the materials. The vial was kept at RT for 5 minutes. After 5 minutes, green gel was formed. After 5 days, the color of the gel was changed gradually from (**gel (green)**) to (**gel (brown)**).

Preparation of hydrogel in inert condition:

8 mL of 25 mM KOH solution was added in a septum capped 50 mL round bottom flask. The solution was purged by N_2 through a needle for 10 min to remove the soluble oxygen from water. After that, desire amount of FcBA and G were added into it and kept under sonication with N_2 purging for 10 min. Then the mixture was heated and stirred by a rice magnetic bid at 80 ℃ for 1 h under N_2. After cooling the solution mixture, the hydrogel was formed.

^{11}B NMR study:

All NMR spectra were recorded at 400 MHz Bruker Advance III 400 NMR. To study ^{11}B NMR experiments, desired amount of ferroceneboronic acid (5.74 mg, concentration = 50 mM in 500 µL) and guanosine (7.08 mg, concentration = 50 mM in 500 µL) were taken into NMR tube. After that, 250 µL of freshly prepared 50 mM KOH in H_2O, 200 µL Milli-Q H_2O and 50 µL of D_2O (final KOH concentration = 25 mM in 500 µL, D_2O = 10% v/v) were added into it. After adding all the components and solvents, NMR tube was heated to solubilize the suspension. After solubilizing the components the tube was kept at room temperature to form gel. After formation of gel, NMR spectra were recorded.

12

UV-visible spectroscopy:

UV-visible absorption spectra were recorded using a Varian Cary 100 Bio spectrophotometer at 298 K. The cell length was 1 cm. Concentration of both gels was 25 mM for this experiment.

Transmission Electron Microscopic experiment:

Transmission electron microscopic (TEM) images were taken using a PHILIPS electron microscope (model: CM 200), with an accelerating voltage of 200 kV. 10% (v/v) of dilute gel solution was dried on carbon-coated copper grids (300 mesh) by slow evaporation in air, then allowed to dry separately under vacuum at room temperature.

Circular Dichroism (CD) study:

Circular dichroism (CD) spectra were recorded at 25 °C on a Jasco J-815 spectropolarimeter. Spectra were measured from 350 nm to 200 nm with a data pitch of 0.1 nm. The bandwidth was set to 1 nm with a scanning speed of 20 nm min^{-1} and a response time of 1 s. The path length was 1 mm quartz cell.

Powder X-ray Diffraction study:

Powder X-ray Diffraction (PXRD) of gels was carried out by Bruker (D2 PHASER) with a wavelength of 1.5406 A˚ at 25 ºC. PXRD studies of corresponding xerogels were performed by placing the samples on the glass plate. X-rays were produced using a sealed tube and X-ray was detected using a linear counting detector based on silicon strip technology (Scintillator NaI photomultiplier detector).

Rheological Measurements:

The rheological study was performed to determine the mechanical properties of the hydrogels by using an Anton Paar Physica Rheometer (MCR 301, Austria) with parallel plate geometry (25 mm in diameter) at a temperature of 25 °C. The dynamic moduli of the hydrogel were measured as a function of frequency in the range of 0.05-100 rad/s with a constant strain value 1%. For thixotropic test, alternative higher and lower strain was set at constant angular frequency of 10 rad/s. The higher strain was 100% and lower strain was 1%. All the experiments were repeated at least three times. For all the experiments, around 200 μL of gel was placed to the geometry plate by using spatula.

Cyclic voltammetry study:

Cyclic voltammogram was recorded on an electrochemical analyzer (Metrohm Autolab potentiostat, Model: PG STAT302N) using glassy carbon as working electrode, saturated

13

Ag/AgCl/KCl (3 M) as reference electrode, Pt wire electrode as counter electrode. The scan rate was 10 mV/s for CV measurements. A solution of tetrabutylammonium hexaflurophosphate in acetonitrile (0.1 M) was employed as supporting electrolyte. 500 µL of the hydrogels were added into 50 mL of electrolyte.

3D printing process:

Printing of hydrogel was carried using INKREDIBLE[+] bioprinter (CELLINK). Printing speed of 10m/s, nozzle diameter of 0.25 mm and pressure of 13KPa were maintained during the printing process. For syringe extruded structures, the gels were put into a syringe and extruded through 22G needle.

Water stability of the hydrogels

100 µL of both gels was taken from vial and placed into PBS buffer (100 mM, 7.4 pH). It was observed that **gel (green)** is hydrophilic and easily soluble. However, **gel (brown)** is hydrophobic and stable in the buffer solution for a month. Gel was gently washed to remove excess gelators before put in solution. The solution was changed after 24h without disturbing the gel.

Acknowledgements

Conflicts of interest

There are no conflicts to declare.

References

[1]   Z. Yang, G. Liang, M. Ma, A. S. Abbah, W. W. Lu, B. Xu, *Chem. Commun*., **2007**, 843.

[2]   H. Cui, B. Xu, *Chem. Soc. Rev*., **2017**, *46*, 6430.

[3]   P. K. Gavel, D. Dev, H. S. Parmar, S. Bhasin, A. K. Das, *ACS Appl. Mater. Interfaces*, **2018**, *10*, 10729.

14

[4]   M. Konda, S. Maiti, R. G. Jadhav, A. K. Das, *Chem. Asian J.*, **2018**, *13*, 204.

[5]   J. Parrish, K. S. Lim, K. Baer, G. J. Hoopera, T. B. F. Woodfield, *Lab Chip*, **2018**, *18*, 2757.

[6]   M. Elsherif, M. U. Hassan, A. K. Yetisen, H. Butt, *ACS Nano*, **2018**, *12*, 2283.

[7]   Y. Koshi, E. Nakata, H. Yamane, I. Hamachi, *J. Am. Chem. Soc.*, **2006**, *128*, 10413.

[8]   A. Biswas, S. Malferrari, D. M. Kalaskar, A. K. Das, *Chem. Commun.*, **2018**, *54*, 1778.

[9]   Z. Huang, P. Delparastan, P. Burch, J. Cheng, Y. Cao, P. B. Messersmith, *Biomater. Sci.*, **2018**, *6*, 2487

[10]   W. Yang, B. Shao, T. Liu, Y. Zhang, R. Huang, F. Chen, Q. Fu, *ACS Appl. Mater. Interfaces*, **2018**, *10*, 8245.

[11]   J. Wang, F. Liu, F. Tao, Q. Pan, *ACS Appl. Mater. Interfaces*, **2017**, *9*, 27745.

[12]   Y. Loo, A. Lakshmanan, M. Ni, L. L. Toh, S. Wang, C. A. E. Hauser, *Nano Lett.*, **2015**, *15*, 6919.

[13]   K. Liu, S. Zang, R. Xue, J. Yang, L. Wang, J. Huang, Y. Yan, *ACS Appl. Mater. Interfaces*, **2018**, *10*, 4530.

[14]   I. Bang, *Biochem. Z.*, **1910**, *26*, 293.

[15]   J. T. Davis, *Angew. Chem. Int. Ed.*, **2004**, *43*, 668

[16]   B. Buchs, W. Fieber, F. V. Elie, N. Sreenivasachary, J. M. Lehn, A. Herrmann, *Org. Biomol. Chem.*, **2011**, *9*, 2906.

[17]   L. E. Buerkle, H. A. von Recumab, S. J. Rowan, *Chem. Sci.*, **2012**, *3*, 564.

[18]   B. Adhikari, A. Shah, H. B. Kraatz, *J. Mater. Chem. B*, **2014**, *2*, 4802.

[19]   G. M. Peters, L. P. Skala, T. N. Plank, B. J. Hyman, G. N. M. Reddy, A. Marsh, S. P. Brown, J. T. Davis, *J. Am. Chem. Soc.*, **2014**, *136*, 12596.

[20]   G. M. Peters, L. P. Skala, J. T. Davis, *J. Am. Chem. Soc.*, **2016**, *138*, 134.

[21]   T. N. Plank, L. P. Skala, J. T. Davis, *Chem. Commun.*, **2017**, *53*, 6235.

[22]   V. Venkatesh, N. K. Mishra, I. R. Canelon, R. R. Vernooij, H. Shi, J. P. C. Coverdale, A. Habtemariam, S. Verma, P. J. Sadler, *J. Am. Chem. Soc.*, **2017**, *139*, 5656.

[23]   A. Pettignano, S. Grijalvo, M. Haring, R. Eritja, N. F. Tanchoux, D. D. Diaz. *Chem. Commun.*, **2017**, *53*, 3350.

15

Accepted Manuscript

[24]   W. L. A. Brooks, B. S. Sumerlin, *Chem. Rev*., **2016**, *116*, 1375.

[25]   A. Abel, Y. Wu, J. Bachmann, *Langmuir*, **2017**, *33*, 8289.

[26]   B. Adhikari, H. B. Kraatz, *Chem. Commun*., **2014**, *50*, 5551.

[27]   B. Adhikari, R. Afrasiabi, H. B. Kraatz, *Organometallics*, **2013**, *32*, 5899.

[28]   M. Ni, N. Zhang, W. Xia, X. Wu, C. Yao, X. Liu, X. Y. Hu, C. Lin, L. Wang, *J. Am. Chem. Soc.*, **2016**, *138*, 6643.

[29]   M. D. S. Maset, V. J. Nebot, J. F. Miravet, B. Escuder, *Chem. Soc. Rev.*, **2013**, *42*, 7086.

[30]   M. E. Garah, R. C. Perone, A. S. Bonilla, S. Haar, M. Campitiello, R. Gutierrez, G. Cuniberti, S. Masiero, A. Ciesielski, P. Samori, *Chem. Commun*., **2015**, *51*, 11677.

[31]   Y. Zhou, X. Ran, A. Chen, Y. Chai, R. Yuan, Y. Zhuo, *Anal. Chem*. **2018**, *90*, 9109.

[32]   S. Aldridge, C. Bresner, I. A. Fallis, S. J. Coles, M. B. Hursthouse, *Chem. Commun.*, **2002**, 740.

[33]   W. L. A. Brooks, B. S. Sumerlin, *Chem. Rev*., **2016**, *116*, 1375.

[34]   M. Bishop, N. Shahid, J. Yang, A. R. Barron, *Dalton Trans*., **2004**, 2621.

[35]   (a) A. S. Batsanov, D. Herault, J. A. K. Howard, L. G. F. Patrick, M. R. Probert, A. Whiting, *Organometallics*, **2007**, *26*, 2414; (b) X. Mo, J. Yakiwchuk, J. Dansereau, J. A. McCubbin, D. G. Hall, *J. Am. Chem. Soc*., **2015**, *137*, 9694.

[36]   T. O. Pennanen, J. Machacek, S. Taubert, J. Vaara, D. Hnyk, *Phys. Chem. Chem. Phys*., **2010**, *12*, 7018.

[37]   A. Ajayaghosh, C. Vijayakumar, R. Varghese, S. J. George, *Angew. Chem. Int. Ed*., **2006**, *45*, 456.

[38]   A. Ajayaghosh, P. Chithra, R. Varghese, *Angew. Chem. Int. Ed*., **2007**, *46*, 230.

[39]   A. Reja, A. Biswas, J. Yadav, D. Dev, A. K. Das, *ChemistrySelec*t, **2017**, *2*, 10984.

[40]   S. Bhattacharjee, S. Bhattacharya, *Chem. Commun.*, **2015**, *51*, 6765.

Graphical Abstract

Redox Active

DYNAMIC G4-QUARTET

3D-Printable

17